Laboratori Nazionali di Frascati

Submitted to Phys. Rev. D

LNF-93/069 (P)
28 Ottobre 1993

N. Fabiano, A. Grau, G. Pancheri:

OBSERVABILITY LIMITS FOR TOPONIUM AT HADRON COLLIDERS

PACS.: 14.80.–j; 12.40.Qq

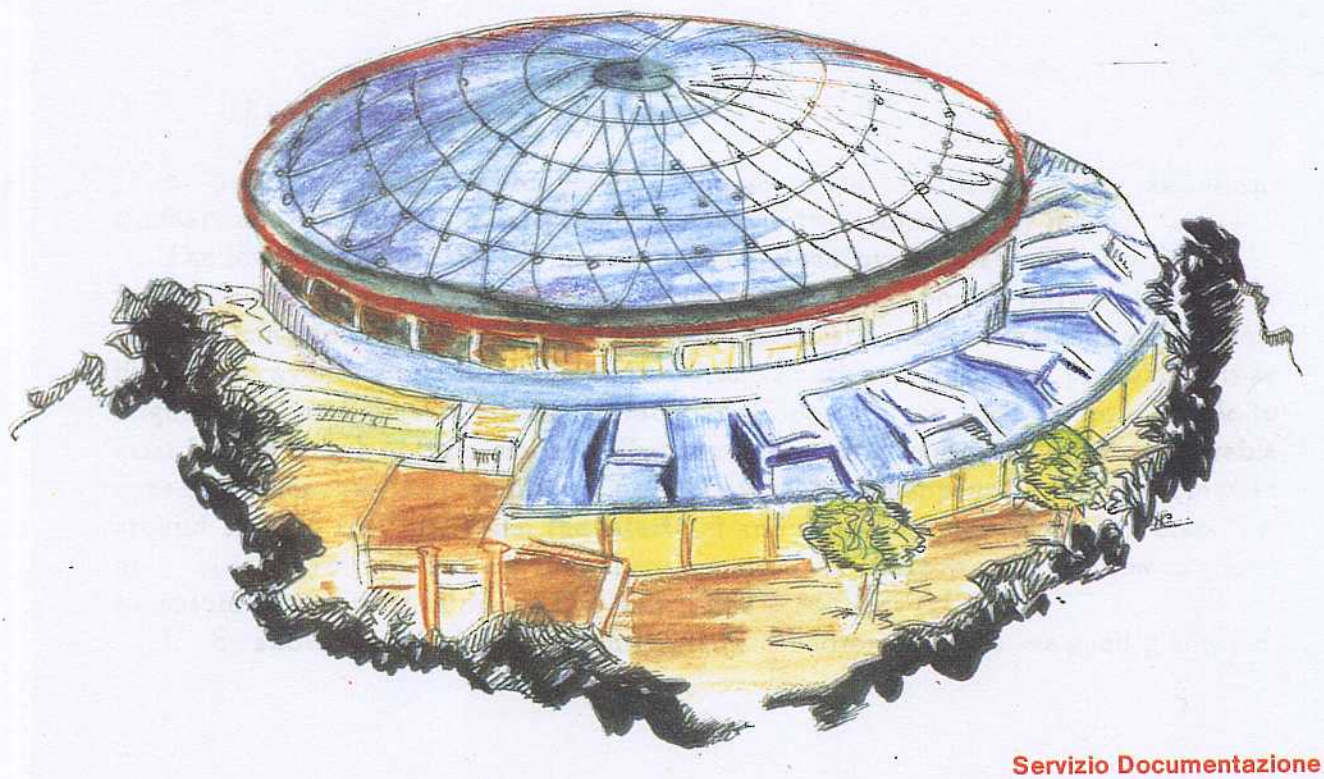

Servizio Documentazione
dei Laboratori Nazionali di Frascati
P.O. Box, 13 - 00044 Frascati (Italy)

ISTITUTO NAZIONALE DI FISICA NUCLEARE - ISTITUTO NAZIONALE DI FISICA NUCLEARE - ISTITUTO NAZIONALE DI FISICA NUCLEARE - ISTITUTO NAZIONALE DI

INFN - Laboratori Nazionali di Frascati
Servizio Documentazione

LNF-93/069 (P)
27 Ottobre 1993

OBSERVABILITY LIMITS FOR TOPONIUM AT HADRON COLLIDERS

N.Fabiano
INFN-Laboratori Nazionali di Frascati, P.O.Box 13, I00044 Frascati ,Italy
A.Grau
Departamento de Fisica Teorica y del Cosmos , Universidad de Granada, Granada, Spain
and
G.Pancheri
INFN-Laboratori Nazionali di Frascati, P.O.Box 13, I00044 Frascati ,Italy
FABIANO@IRMLNF, 16487::IGRAU, PANCHERI@IRMLNF

Abstract

We discuss existency conditions for toponium bound states and estimate the wave function at the origin, comparing different models for the static interquark potential. We evaluate the production cross-section for the singlet state with $J^{PC} = 0^{-+}$, and compare the signal with the expected QCD background at SSC energies. We find that the present lower limits on the top mass almost exclude the possibility of these bound states and their detectability.

1 Introduction

In this paper, we study the production of toponium states with $J^{PC} = 0^{-+}$ at hadron colliders and their possible detection through the two photon decay mode.

The lower limits on the top quark mass obtained by the CDF Collaboration [1] , i.e. $m_t \geq m_W + m_b$, have drastically changed the familiar bound state picture which charmonium and bottomium spectroscopy had established, since the top quark can now directly decay into a real W-boson and a bottom quark and this decay probability is as large as the one typical of strong interactions. Toponium can then be too unstable to exist for any length of time, since its life-time is becoming so short as to be comparable or even smaller than the revolution time[2]. Typically this happens for top quark masses around 130-150 GeV/c^2. From the latest D0 and CDF [3] limits on the top mass, i.e. $m_t \geq 113\ GeV/c^2$, we then see that there remain a very narrow mass window in which toponium can exist at all, i.e. $220 \leq m_{t\bar{t}} \leq 260 \div 300\ GeV/c^2$.

In the above energy range, presently planned hadron colliders are good gluon fac-

tories and gluon-gluon fusion is the most abundant production mechanism for quark-antiquark bound states. As for the decay channel, at hadron colliders bound states have traditionally been identified through their leptonic or electromagnetic decays, in order to overcome the large hadronic backgrounds. In [4], it has been suggested to search at LHC for the state $J^{PC} = 0^{-+}$ in the two photon decay mode. An estimate of the statistical significance, using realistic LHC type detectors, was done to show that observability of η_t was possible for toponium masses in the $200 \div 240$ GeV/c^2 mass range. The calculation of the signal cross-section is however very sensitive to the estimate of $|\Psi(0)|$, the wave function at the origin for the bound state. Indeed, the signal cross- section is proportional to the fourth power of the wave function, since $\sigma \approx \Gamma_i \Gamma_f / \Gamma_{tot}$. While both Γ_i and Γ_f (decay width into initial and final state channels) are proportional to $|\Psi(0)|^2$, the total decay width for toponium is dominated by the electroweak single quark decay, which is independent from the value of the wave function at the origin. This is a totally novel situation, quite different from all the other quarkonia states : an uncertainty of as much as 30% on the wave function will produce a difference by more than a factor 4 on the number of observed events. Thus, in [5], the effects of QCD-inspired potential models and that of higher order QCD corrections have been used to obtain a signal cross-section which is a factor 4 to 10 lower than the one in [4]. For this case, the observability of the $\eta_t \rightarrow \gamma\gamma$ signal at LHC is out of question, except for the case $m_{t\bar{t}} \approx 100$ GeV/c^2 (a possibility now excluded by present experiments [3]) .

In this paper we discuss and compare the different values for the wave function at the origin, obtained from different potential models. In particular, we compare results from a static Coulomb potential, with a one and two loops expression for the strong coupling constant α_s with the QCD potentials, which typically use a running α_s evaluated at the two loops level. We see that the use of the two loops expression for both Coulomb and QCD potentials produces very similar results for $|\Psi(0)|$, independently of the fact that in the Coulomb case α_s is not running. Thus, a good estimate can be done just using the Coulomb potential in a hydrogen like model, which allows for intuitive and simple estimates.

We then compare the resulting estimates for the production cross-section with the expected irreducible QCD background, both at LHC as well as at higher energies. At SSC energies, we notice that there is no significantly discernible signal for toponium in the mass range given above with an expected luminosity $L = 10^{33} cm^{-2} sec^{-1}$. Even if the high luminosity option [6] $L = 10^{34} cm^{-2} sec^{-1}$ is considered, the signal to noise ratio is acceptable only for toponium masses up to 260 GeV/c^2, for the more singular one loop Coulomb-type potential, and up to $\approx$ 220 GeV/c^2 for the so-called QCD potentials.

It then appears that the possibility of observing the process

$$gluon\ gluon \rightarrow \eta_t \rightarrow \gamma\gamma$$

is rather small, although it cannot be excluded yet. We stress, however, the importance

of looking for this type of processes: the sensitivity of the cross section to the interquark potential renders it a unique probe of the complete QCD bound state picture.

In Sect.2 we discuss the existency conditions for toponium by comparing different potential model estimates for the $1S - 2S$ splitting with the total toponium decay width. In Sect.3, we present an estimate of the toponium wave function at the origin for a set of potential model predictions and evaluate electromagnetic decay widths and Branching Ratios for the one loop Coulombic case. With these widths, we calculate the signal cross section into two photons for the Coulombic type potential, in the narrow width approximation and to the Born level in the parton densities. In Sect. 4 we discuss the irreducible QCD background, for various kinematic cuts. In Sect. 5 the signal is folded with the experimental resolution for an optimized gamma detector and compared to the expected background, in order to evaluate the statistical significance of the signal. This is done both for the Coulomb case as well as for the less singular QCD potentials, at SSC energies.

2 Existency Conditions

For a top quark with $m_t \geq m_W + m_b$, the total decay rate for a quark-antiquark bound state is dominated by single quark decay into a W boson and a b quark [2, 7]. This decay rate is an increasingly large function of the top quark mass, or in other words, the lifetime of the top quark becomes shorter and shorter as its mass becomes larger. As this happens the toponium width becomes dominated by single quark decay and, for high top masses we can assume $\Gamma_{t\bar{t}} \simeq 2\Gamma_t$. When the decay width overtakes the level splitting between the bound states, no formation of the bound state is envisaged, and the top quark decays before completing a revolution. While the single quark decay width is fully determined from electroweak interactions through the expression

$$\Gamma(t \to Wb) = \frac{G_F m_t^3}{8\pi\sqrt{2}} \left(\frac{2p}{m_t}\right) \left[\left(1 - \frac{m_b^2}{m_t^2}\right)^2 + \frac{m_W^2}{m_t^2}\left(1 + \frac{m_b^2}{m_t^2}\right) - 2\frac{m_W^4}{m_t^4}\right] \sim \frac{m_t^3}{16\pi(246\ GeV)^2} \tag{1}$$

with p the W-boson momentum in the t-quark rest frame, the splitting between the energy levels of the bound states depends upon the strength of the strong force between the quarks and their relative distance[8]. For light quarks one can expect long range confining forces to be dominant, whereas for the top quark the Coulomb part of the potential, i.e.

$$V_Q = -\frac{4}{3}\frac{\alpha_S}{r} \tag{2}$$

should be the dominant one[9]. Corrections for Higgs boson exchange Yukawa type forces can also be expected[10, 11], but, for a top quark with mass less than $\approx 200\ GeV$, they are small, with an attractive potential for the quark-antiquark singlet state, and may amount to no more than 10% of the Coulomb term. On the other hand, higher

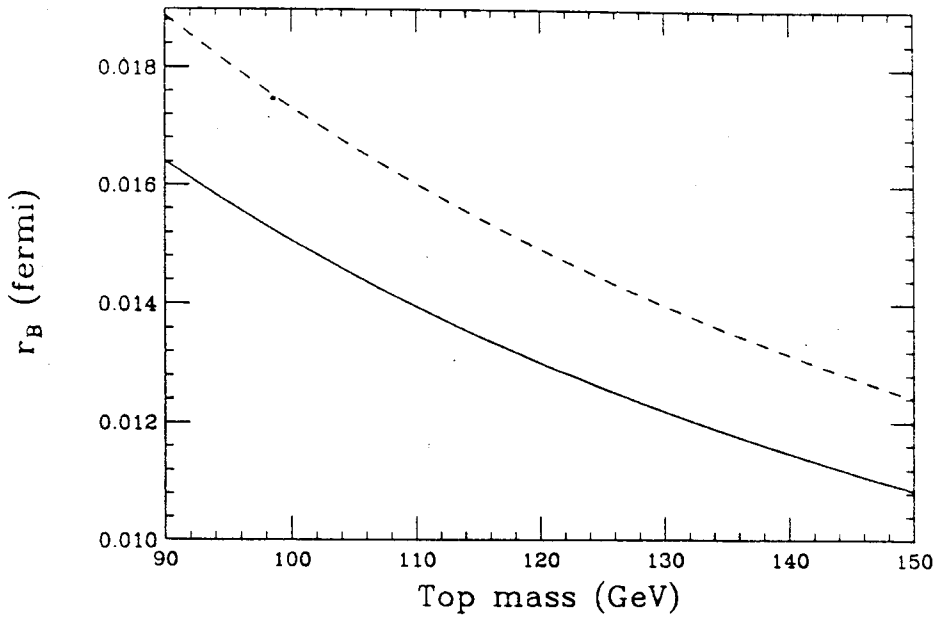

Figure 1: Bohr Radius for Coulombic potential , vs. top mass, for one (full line) and two loop (dashes) α_s, with $N_F = 5$, $\Lambda_{\overline{MS}} = 0.2\ GeV$.

order QCD corrections to the potential can be included in α_s through its two loops expression, as shall be discussed in what follows.

To begin with, it is instructive to discuss the top-antitop bound states using a Coulomb potential with QCD couplings and α_s evaluated at a fixed distance r, which can be plausibly chosen to be the Bohr radius of the bound state. In this case, the non-relativistic Schroedinger equation can be exactly solved[8] and one can easily evaluate binding energies and the wave function at the origin. The use of a non-relativistic treatment can be justified because the presently rather high limits on the top mass imply for the heavy quark velocity $\beta_Q \approx \alpha_s(M^2_{Q\bar{Q}}) \approx 0.1 \div 0.2$. Then the relativistic corrections, which are of order β^2_Q, can be expected to be $\approx 1 \div 4\%$. Treating the top-antitop system as a non-relativistic hydrogen atom, with a non-running (in r) coupling constant for the potential, allows for the use of analytical formulae, from which estimates for decay rates and production cross-sections can be extracted immediately. As we shall see later, the use of the Coulombic potential gives results similar to those with a running (in r) α_s, for the case in which a two loop α_s is used.

For the Coulombic type potential with a non running α_s, the energy levels are given by

$$E_n = -\frac{4}{9n^2} m_t \alpha_s^2 \tag{3}$$

and the Bohr radius of the state is given by

$$r_B = \frac{3}{2\alpha_s m_t} \tag{4}$$

Then, the scale at which to evaluate α_s can be extracted from the above equation with $\alpha_s = \alpha_s(1/r_B)$. In fig.1 we show r_B as a function of the top quark mass and using both the one and the two loops expression for α_s, i.e.[9, 12]

$$\alpha_s^{(1)} = \frac{4\pi}{b_0 log[(1/r_B\Lambda_{\overline{MS}})^2]} \quad and \quad \alpha_s^{(2)}(r) = \frac{4\pi}{b_0 f(r)}\left\{1 + \frac{c}{f(r)} - \frac{b_1}{b_0^2}\frac{\log[f(r)]}{f(r)}\right\} \tag{5}$$

with

$$f(r) = \log\left[\frac{1}{(\Lambda_{\overline{MS}}r)^2} + b\right], \quad c = \frac{1}{b_0}\left(\frac{93 - 10N_f}{9}\right) + 2\gamma_E \tag{6}$$

$$b_0 = 11 - \frac{2}{3}N_f, \quad b_1 = 102 - \frac{38}{3}N_f \tag{7}$$

where $\Lambda_{\overline{MS}}$ is the QCD constant and N_f the number of flavours.

With the values for α_s extracted from the figure, one can now calculate the level splitting for the Coulombic potential and compare it both with the splitting from various potential models , as well as with the toponium width.

The potentials we have considered can be grouped in four types:

1. Cornell type potential:

$$V(r) = -\frac{k}{r} + \frac{r}{a^2} \tag{8}$$

with parameters $a = 2.43$, $k = 0.52$ (case A), and $a = 2.09$, $k = 0.3$ (case B). This potential [13] is as singular as the Coulombic one and its strength at the origin is close to the one obtainable from the one loop expression.

2. Richardson potential [14]:

$$V_R(r) = -\frac{4}{3}\frac{12\pi}{33 - 2N_f}\int \frac{d^3q}{(2\pi)^3}\frac{e^{iqr}}{q^2\log(1 + q^2/\Lambda^2)} \tag{9}$$

$N_f = 3$ and $N_f = 5$, $\Lambda = 398\ MeV$.

3. QCD inspired potential V_J of Igi-Ono [15, 16]:

$$V_J(r) = V_{AR}(r) + dre^{-gr} + ar, \quad V_{AR}(r) = -\frac{4}{3}\frac{\alpha_s^{(2)}(r)}{r} \tag{10}$$

with the parameter set [17]:

Parameters	$N_f = 4, \quad b = 20$		
$\Lambda_{\overline{MS}}\ (GeV)$	0.2	0.3	0.5
$a\ (GeV^2)$	0.1587	0.1443	0.1391
$d\ (GeV^2)$	0.2550	0.0495	1.476
$g\ (GeV)$	0.3436	0.3280	2.955

We have also used the same set of parameters a, d and g as above with $N_f = 5$, which could be more appropriate for the large masses under consideration. The value $\Lambda_{\overline{MS}} = 0.366\ GeV$, has also been used, with a, d and g parameters as for the $\Lambda_{\overline{MS}} = 0.5\ GeV$ case above. The conventional definition for $\Lambda_{\overline{MS}}$ requires it to be dependent upon N_f, and the relationship between the different $\Lambda_{\overline{MS}}(N_f)$ are obtained by using the continuity of α_s at quark masses [12].

4. Power law, Martin-type Potentials [18, 19, 20],

$$V(r) = -8.064 + 6.8698\ r^{0.1} \tag{11}$$

recently revisited by Rosner et al.[21]:

$$V(r) = \frac{\lambda}{\alpha}(r^{\alpha} - 1) + c \tag{12}$$

The parameters assume the values $\alpha = -0.14$, $\lambda = 0.808$, $c = -1.305$ (case A), and $\alpha = -0.12$, $\lambda = 0.801$, $c = -0.772$ (case B). In Fig. 2 we show the toponium width, $\Gamma_{t\bar{t}} = 2\ \Gamma_t$ together with the level splitting for the various potential models, as indicated [22].

For low quark masses, the states are well separated and the splitting is larger than the electroweak decay width. However, since the splitting grows linearly with the top mass, whereas the decay width grows like m_t^3, there will be a mass value where the decay width "takes over" the splitting. If we assume as existency condition

$$\Delta E_{2S-1S} \geq \Gamma_{t\bar{t}} \tag{13}$$

we see from fig.2 that formation of the bound state is possible for top quark masses less than 130–150 GeV. This is shown in the figure for a selection of currently proposed potentials.

3 Decay Width, Branching Ratios and Production Cross-section

Given the experimental limits on the top mass, in what follows we shall illustrate the problem at the Born level. If the higher order corrections become too large, an

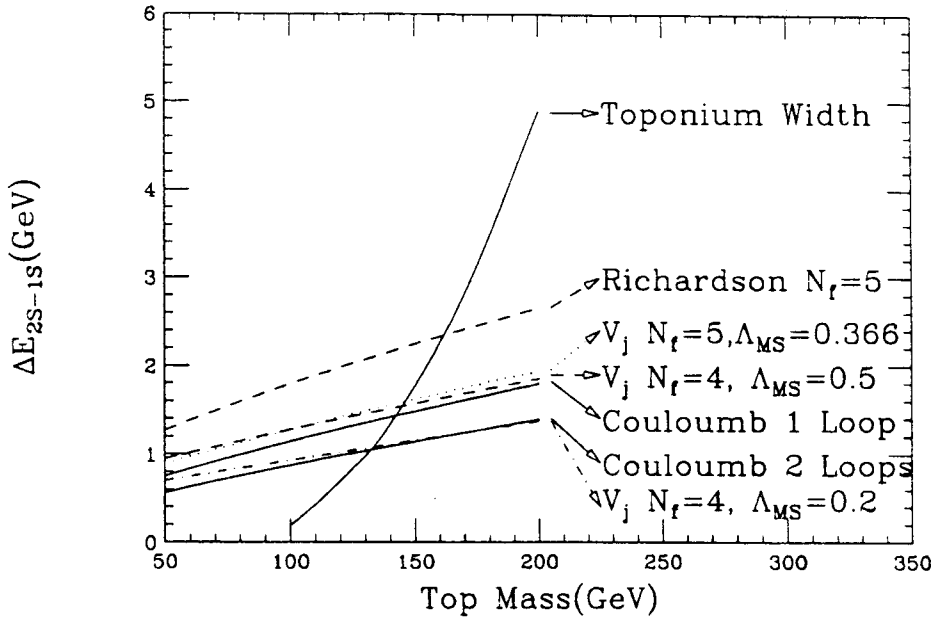

Figure 2: Energy splitting (full lines) for a Coulomb type potential in the Non relativistic Hydrogen like model described in the text, together with other models, compared to toponium width (full line), vs. top mass.

altogether different (presumably non-perturbative) approach should be used. The state we discuss here, as well as throughout the paper, is $J^{PC} = 0^{-+}$ with special focus on the electromagnetic decay width. At future large hadron colliders the main production mechanism is through gluon-gluon fusion, as in the case of Higgs production, where, for relatively low mass values, production is dominated [23] by gluonic processes. For η_t final state, decay channels include [17, 24] vector boson combinations like WW, ZZ, HZ, γZ, $\gamma\gamma$, gluon gluon and all the fermion-antifermion pairs. Of interest here are the decay into two photons[25] or two gluons, for which the following Born level expressions hold (m is the toponium mass):

$$\Gamma_B(\eta_t \to \gamma\gamma) = 12 e_t^4 \alpha^2 \frac{4\pi|\Psi(0)|^2}{m^2} \tag{14}$$

and

$$\Gamma_B(\eta_t \to gg) = \frac{8}{3}\alpha_s^2 \frac{4\pi|\Psi(0)|^2}{m^2} \tag{15}$$

where $|\Psi(0)|$ is the wave function at the origin. Notice, that higher order radiative corrections are expected to reduce these expressions [26] as follows:

$$\Gamma(\eta_t \to \gamma\gamma/gg) = \Gamma_B \left[1 + \frac{\alpha_s}{\pi}\left(\frac{\pi^2}{3} - \frac{20}{3}\right)\right], \tag{16}$$

where Γ_B is the Born level decay width . At the Born level, the Coulombic potential (non-relativistic case) gives for the wave-function at the origin

$$|\Psi_{100}(0)|^2 = \frac{1}{\pi}\left(\frac{2}{3} m_Q \alpha_s\right)^3 \tag{17}$$

where m_Q is the mass of the heavy quark. For η_t the branching ratios into two photons and into two gluons are then obtained from

$$\Gamma_B(\eta_t \to \gamma\gamma) = \frac{256}{729}\alpha^2 \alpha_s^3(Q_s^2) m \tag{18}$$

$$\Gamma_B(\eta_t \to gg) = \frac{32}{81}\alpha_s^2(Q_h^2)\alpha_s^3(Q_s^2) m \tag{19}$$

and from eq.(1) with the toponium width, $\Gamma_{t\bar{t}} = 2\Gamma_t$. In the above equations, we distinguish between a soft and a hard scale, which correspond respectively to the soft gluonic exchanges between the bound quarks and the hard annihilation into two gluons, for which the scale of α_s is of the order of the final state energy. Following the prescription for the argument of α_s given in the previous section, we can write

$$Q_s^2 = \frac{1}{r_B^2} = m_t E_1 \qquad Q_h^2 = m^2 \tag{20}$$

We now report in Table 1 the values obtained in the Coulomb model, using the one-loop expression for α_s and $\Lambda = 0.2\ GeV$.

Table 1

m_t GeV	$\Gamma_{t\bar{t}}$ GeV	$\alpha_s(Q_s^2)$ $Q_s^2 = m_t E_1$	$\alpha_s(Q_h^2)$ $Q_h^2 = m^2$	$\Gamma(\eta_t \to gg)$ MeV	$\Gamma(\eta_t \to \gamma\gamma)$ KeV	$B.R.(\eta_t \to \gamma\gamma)$ –
100	0.187	0.196	0.119	8.4	32	1.73×10^{-4}
110	0.390	0.192	0.117	8.4	33	0.85×10^{-4}
120	0.650	0.189	0.116	8.6	35	0.53×10^{-4}
130	0.970	0.187	0.115	8.7	36	0.38×10^{-4}

The estimates shown in Table 1 are very sensitive to the wave function at the origin, which depends upon the choice of potential. As one can see already from Fig.2, the use of the one or two loops expression for α_s in the Coulomb-type potential can give rather different results. Although, in principle, one should already be in a region of Q^2 where α_s is small enough for a perturbative calculation, the photonic decay width has an α_s dependence to the cubic power and this can result in rather different predictions for the widths.

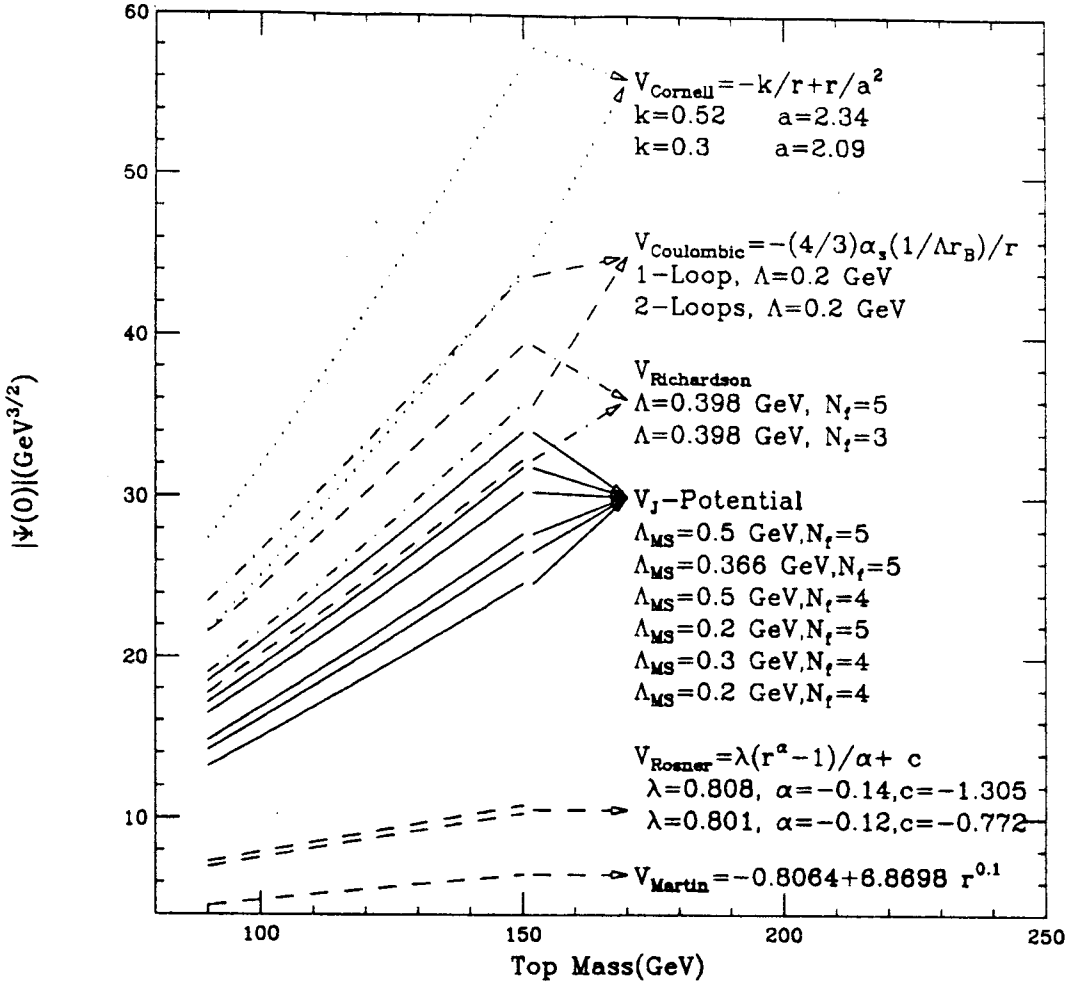

Figure 3: $|\Psi(0)|$ versus top mass for different potential models as indicated in the figure.

A quantitative description of the dependence upon the choice of the potential is shown in Fig.3, where we have calculated $|\Psi(0)|$ for the models described in the previous section.

We shall now proceed to calculate the production cross-section at hadron colliders. For a narrow $J = 0$ resonance produced through gluon-gluon fusion, the following delta function expression can be used

$$\sigma(pp \to \eta_t + X) = \frac{\pi^2}{8m^3}\Gamma(\eta_t \to gg)\left(\tau \int_\tau^1 \frac{dx}{x} g(x,Q^2) g(\frac{\tau}{x},Q^2)\right) \qquad (21)$$

with $\tau = m^2/s$. If there are many narrow bound states, following [27], the wave function at the origin, which enters into the above expression through the width into gluons, can be replaced as follows

$$|\Psi_{100}(0)|^2 \to \sum_n |\Psi_{n,0,0}(0)|^2 \approx |\Psi_{100}(0)|^2 \zeta(3) \tag{22}$$

with

$$\zeta(3) = \sum_n \frac{1}{n^3}$$

Inserting into eq.(21) the formula from eq.(15), one obtains an expression identical to the one obtained in [27] in the narrow width approximation, i.e.

$$\lim_{\frac{\Gamma}{M}\to 0} \sigma_{FKS} = \frac{\pi^2 \alpha_s^2}{6s} \left(\frac{p_s}{m_t}\right)^3 \zeta(3) \left(\frac{dL}{d\tau}\right)_{gg} \tag{23}$$

with

$$p_s = \frac{2}{3} m_t \hat{\alpha}_s \qquad \hat{\alpha}_s = \alpha_s(m_t E_1) \tag{24}$$

which is in fact the exact solution for the Coulomb potential. Indeed, in [27], the argument for α_s is given as

$$Q^2 = m_t \sqrt{E_1^2 + \frac{\Gamma_{t\bar{t}}^2}{4}} \simeq m_t E_1 \tag{25}$$

As previously discussed, this value of Q^2 is the non–relativistic momentum of a quark of mass m_t in a bound state, when one takes into account reduced mass and finite width effects.

Clearly the use of the one or two loops expression for α_s makes a remarkable difference, since α_s, evaluated at the soft scale from the wave function calculation, now enters to the sixth power and an initial difference of 10 % is amplified to become a factor 6. Thus, even higher order terms are not negligible for a precise evaluation. To establish lower and upper limits for detectability, one can start with the one loop expression.

A numerical evaluation of the cross-section at LHC energies [4, 27, 28] indicates the possibility of detection only if the top quark has a mass around 100-120 GeV. In fact the total production cross-section, $\approx$ 100 pb , with a 10^{-4} branching ratio into two photons, leads to about 1000 events for an integrated LHC luminosity of $10^2 fb^{-1}$. At SSC energies, the cross-section is a factor 3 larger, but this advantage can be lost if the expected luminosity in one year of running is only 10 fb^{-1}. Even if the number of events were acceptable, however, the observability of a possible signal crucially depends on the physics background, to which we turn in the next section.

4 QCD Background

The irreducible QCD background to the two photon decay channel comes from three possible processes, the Born term, i.e. $q\bar{q} \to \gamma\gamma$, the box diagrams [29, 30] *gluon gluon* $\to$

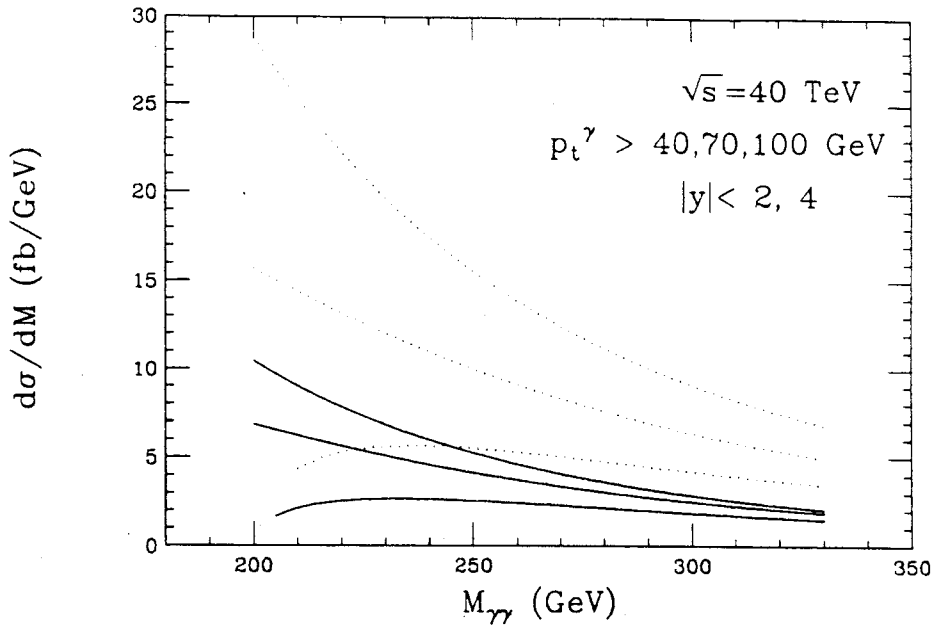

Figure 4: Differential cross-section for $q - \bar{q}$ annihilation to two photons, with rapidity cut on each photon $|y| \leq 2$(full) and 4 (dots), and different transverse momentum cuts, $p_t^{\gamma} \geq 40, 70$ and 100 GeV. Densities are HMRSB type[32].

$\gamma\gamma$, and the bremsstrahlung contributions [31]$qg \to q\gamma\gamma$.

In the above processes, the Born and the bremsstrahlung terms have singularities for small transverse momentum of the emitted photons, which make them quite larger (by as much as one order of magnitude) than the signal. To reduce the background, one must impose kinematic cuts both in rapidity as well as on the photon transverse momentum. In Fig.4 we show the differential cross-section for the annihilation process, and for different cuts on the photon transverse momentum. The effects of rapidity cuts, $y \leq 2, 4$ are also shown.

The kinematic cuts have the effect of reducing the Born term contribution to a few femtobarn per GeV. This cross-section is now comparable to the one obtainable from the signal. We have in fact seen in the previous section, that in the top mass range around 100 GeV, the signal can be estimated to give a cross-section $\approx 10 - 20 fb$.

The other important background contribution comes from gluon-gluon fusion into two photons. In the mass range of interest, this process, at LHC/SSC energies, will give a contribution of the same order of magnitude as the annihilation. The large gluon densities in fact compensate for the extra powers in α_s and make mandatory the inclusion of these contributions. For this process, the dependence of the amplitudes from the internal quark masses has been discussed in [30].

In Fig. 5, we have fixed the top mass to be 110 GeV, so as to evidentiate how this contribution depends upon the kinematic cuts. Then, for a specific set of cuts, we

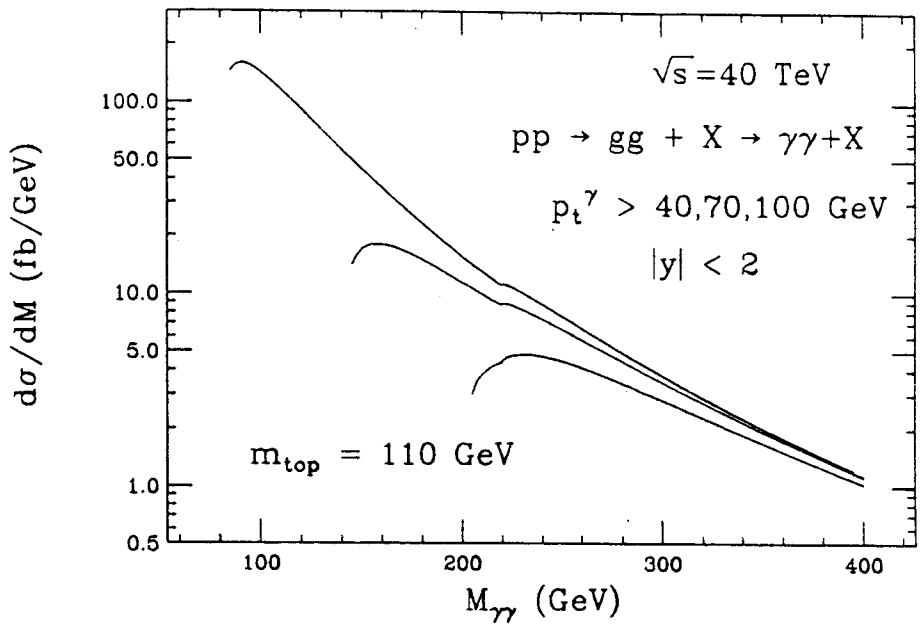

Figure 5: Differential cross-section from the box diagram contribution to $\gamma\gamma$ production, with HMRSB type densities[32].

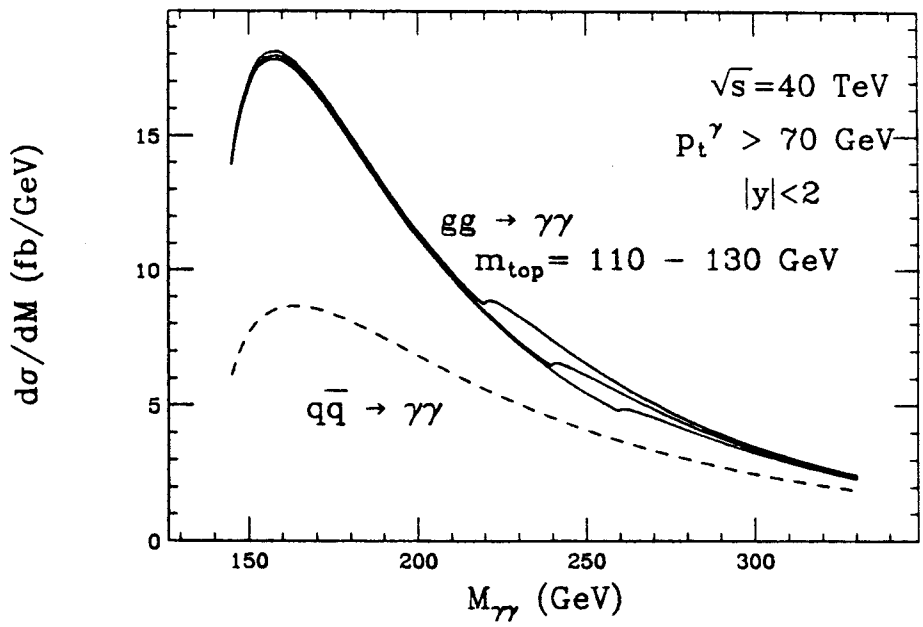

Figure 6: Differential cross-section for two photon production from initial gluon-gluon processes, for different values of the internal heavy quark mass, as indicated (full lines), and from the $q\bar{q}$ contribution (dashed line). Densities are from HMRSB [32].

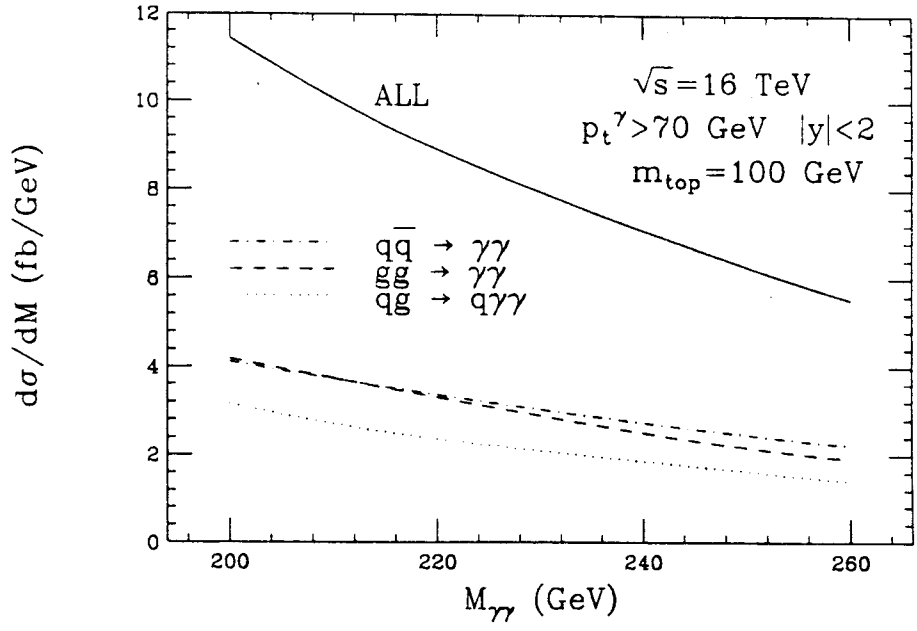

Figure 7: Individual contribution and sum of irreducible QCD background terms at LHC. Densities are from [32].

have let the internal heavy quark mass vary. This is illustrated in Fig. 6.

The bremsstrahlung diagrams which contribute to the background are quite a few [31]. To obtain an estimate of this contribution, we calculated the different background cross-sections at LHC and compared with an estimate by C.Seez. [33]. The contribution of all three sources of background at LHC is shown in fig.7, where, as far the bremsstrahlung term is concerned, transverse momentum cut as well as an isolation cut are imposed. We notice that at LHC, the bremsstrahlung contribution is close to the one from quark-antiquark annihilation, if the same cuts are applied.

At SSC energies, we have then taken the bremsstrahlung contribution after cuts to be the same as the one from gluon-gluon fusion. The total background contribution one can expect from the above irreducible processes at SSC energies, is then shown in Fig. 8. The kink in the cross-section, noticeable around a top quark mass at 110 GeV come from the box diagram for an internal 110 GeV top mass. Since we have taken the bremsstrahlung part to be as large as the one from the box diagram, the bump appears in the sum as well.

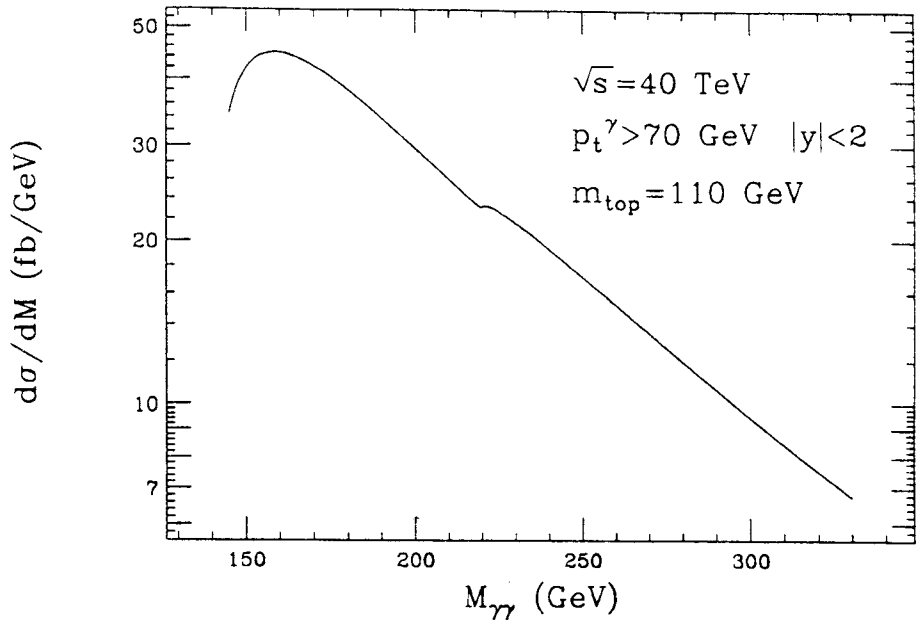

Figure 8: Differential cross-section for two photon production (other than toponium), with densities from HMRSB [32].

5 Signal Cross-section for $pp \to \gamma\gamma + X$ and statistical significance

In order to estimate the signal cross section for the process

$$pp \to \eta_t + X \to \gamma\gamma + X$$

one needs to take into account the experimental resolution for the possible gamma gamma detectors. In general, one has

$$\frac{d\sigma}{dM} = \frac{(\sigma_\eta \cdot BR)}{\sqrt{2\pi}\sigma_G} \cdot \exp\left[-(M - m_{t\bar{t}})^2/2\sigma_G^2\right], \tag{26}$$

where $\sigma_\eta \cdot BR$ is the total production cross-section in the given final state with branching ratio BR. The gaussian width σ_G is the sum in quadrature of the natural width and the experimental resolution, i.e. $\sigma_G = \sqrt{\sigma_{nat}^2 + \sigma_{exp}^2}$ where $\sigma_{nat} = \frac{\Gamma_{t\bar{t}}}{2.35}$ and σ_{exp} is the experimental resolution, which depends upon the calorimeter used in the detection. We assume the particular conditions described in [23, 33], with an experimental resolution given by

$$\frac{\Delta E}{E} = \frac{0.02}{\sqrt{E}} \quad \textit{with a constant term } \frac{1}{2}\% \tag{27}$$

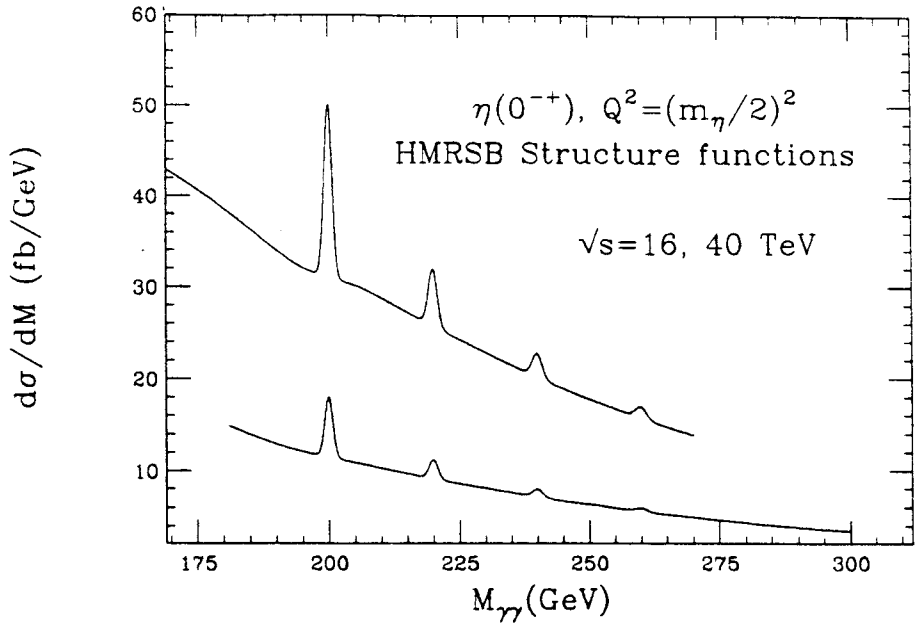

Figure 9: Differential cross-section for two photon production at LHC and SSC energies, with rapidity cut on each photon $|y| \leq 2$ and transverse momentum cut $p_t^\gamma \geq 70\ GeV$.

and show in Fig. 9 the results we obtain for different values of the top mass. The signal cross section of this figure includes both background and signal, for the one loop Coulomb model, for SSC energies and LHC, respectively. We notice that the clear peak at $m_{top} = 100\ GeV$ is now excluded by the recent CDF [3] limits and possible searches for this state can only concentrate on the higher mass values. Notice also, as discussed previously, that a two-loop Coulomb model will give cross-sections and branching ratios such that the peak values will be reduced by at least a factor 4. For such potentials, the observability of the signal, even for the higher mass values, will then disappear. The signal cross-section shown in the figure has been computed with the experimental resolution of eq.(27), with

$$\sigma_G = \Delta m_{\gamma\gamma} \approx \sqrt{2}\Delta E \text{ and } \Gamma_{t\bar{t}} = 2\Gamma_t$$

As discussed in [4], the experimental resolution dominates the signal width for low values of the top quark mass. For a heavier top, $\approx 120\ GeV/c^2$ and above, the two become comparable and the signal becomes more and more diffuse, as the single top decay width becomes larger and larger.

One can evaluate the statistical significance for this signal at SSC energies, by plotting the signal level above noise $S = N_{signal}/\sqrt{N_{signal} + N_{bck}}$. For the signal, the number of events is estimated by taking all the events around the resonance peak,

within a mass bin $\Delta M = \Gamma_{t\bar{t}}$. This amounts to 85 % of the peak cross-section. The number of background events contained in the same mass bin is then obtained from

$$N_{bck} \simeq \frac{d\sigma}{dM}|_{m_{t\bar{t}}} \cdot 3\sigma_G \tag{28}$$

where σ_G is the gaussian width.

As pointed out in [5], for the case of the V_J–potential the signal is reduced by at least a factor 4, relative to the one–loop Coulomb potential case discussed in [4], so that at LHC for a luminosity of $10^{34} cm^{-2} sec^{-1}$ and $\Delta t = 10^7\ sec$, the signal will remain below the noise level for any acceptable value of the top mass. At $\sqrt{s} = 40 TeV$, the situation, at least for the low luminosity option $L = 10^{33}\ cm^{-2}\ sec^{-1}$, is even worse: the background and signal increase by a factor $\approx 2 - 3$, but the luminosity would be smaller by a factor 10 and the observability limit would be reached earlier. Only a high luminosity option, [6], i.e. $L = 10^{34}\ cm^{-2}\ sec^{-1}$, could leave some window of detectability. It should be noticed that, even in this case, it is not clear as to whether it would be possible to obtain the extreme conditions described previously for the experimental apparatus.

For a possible high experimental resolution case, we nonetheless show, in Fig. 10, the signal to noise ratio at SSC, with two different luminosity options, using for the signal cross section two different potential models, the one-loop Coulomb model and the most optimistic case for the V_J potential (which is very similar to the two loop Coulomb potential).

6 Conclusions

The possibility of observing toponium bound states at LHC and SSC energies has been discussed for different luminosity options, and for a very precise detector configuration. The sensitivity of the signal cross-section from the interquark potential has been highlighted. It appears that present limits on the top mass, almost but all exclude the possibility of formation and subsequent detection of the bound states.

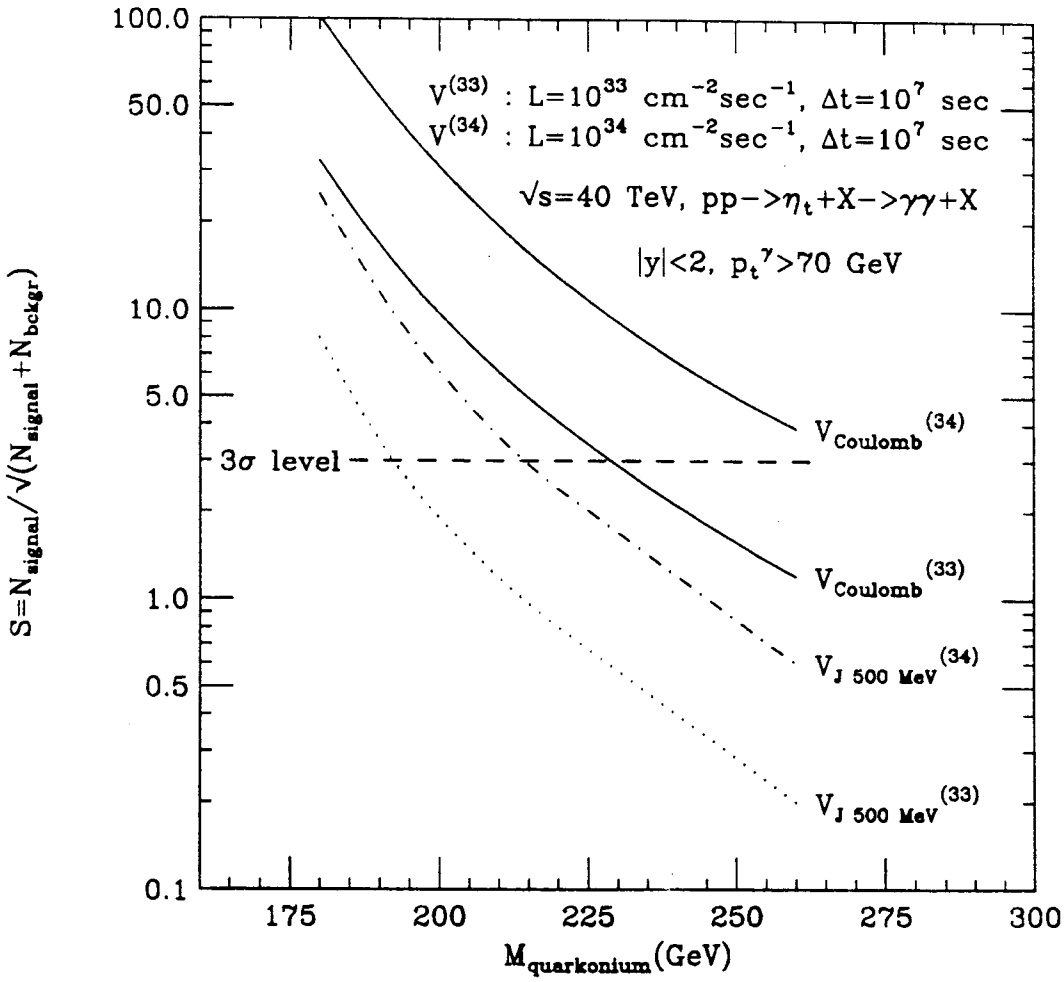

Figure 10: Number of Standard Deviations at SSC with one-loop Coulomb and V_J potential, for different machine luminosities.

References

[1] CDF Collaboration, F. Abe et al., *Phys Rev. Lett.* **64** (1990) 142, 147; ibidem **68** (1992) 447.

[2] I.Bigi, Y.Dokshitzer, V.Khoze, J.Kuhn and P. Zerwas, *Phys. Lett.* **B181** (1986) 157.

[3] CDF Collaboration, P.Tipton, *Top Search at CDF*, XXVII International Conference on High Energy Physics, Ithaca August 1993.
D0 Collaboration, N. Hadley *Top Search at D0*, XXVII International Conference on High Energy Physics, Ithaca August 1993.

[4] G.Pancheri, J.-P. Revol and C.Rubbia, *Physics Letters* **B277** (1992) 518.

[5] J. H. Kuhn and E. Mirkes, *Physics Letters* **B296** (1992), 425; J. H. Kuhn and E. Mirkes, Phys. Rev D48 (1993)179.

[6] R. Schwitters, *Future Hadron Colliders: The SSC*, XXVI International Conference on High Energy Physics, August 6-12 1992, Dallas, Texas.

[7] V. Barger, H. Baer, K.Hagiwara and R. J. N. Phillips, *Phys. Rev.* **D30** (1984) 947.

[8] V. S. Fadin, V. A. Khoze, *JEPT Lett.* **46** (1987) 525; *Yad. Fiz.* **48** (1988) 487.

[9] A.Billoire, *Phys. Lett.* **B92** (1980) 343.

[10] H. Inazawa and T.Morii, *Phys. Lett.* **203B** (1988) 279.

[11] M.J.Strassler and M.E.Peskin, *Phys.Rev.* **D43** (1991) 1500.

[12] W.A.Bardeen, A.J.Buras, D.W.Duke and T.Muta, *Phys. ReV.* **D18** (1978) 3998; W.J. Marciano, *Phys. Rev.* **D29** (1984) 580.

[13] E. Eichten, K. Gottfried, T. Kinoshita, K. D. Lane, T. M. Yan, *Phys. Rev.* **21D** (1980) 203.

[14] J.L. Richardson, *Phys. Lett.* **82B** (1979) 272.

[15] J.H.Kuhn and S.Ono, *Zeit Phys.* **C21** (1984) 385; K.Igi and S.Ono, *Phys. Rev.* **D33** (1986) 3349.

[16] W.Buchmuller and S.-H.H.Tye, *Phys. Rev.* **D24** (1981) 132.

[17] J. H. Kuhn and P. Zerwas, *Phys. Rep.* **167** (1988) 321, and references therein.

[18] A. Martin, *Phys. Lett.* **93B** (1980) 338 and *Phys. Lett.* **100B** (1981) 511.

[19] M. Mahchacek, Y. Tomozawa, *Ann. Phys. (NY)* **110** (1978) 407.

[20] C. Quigg, J. Rosner, *Comments Nuclear Particle Physics* **8** (1978) 11.

[21] A. K. Grant, J. L. Rosner, E. Rynes; *Phys. Rev.* **D47** (1993) 1981.

[22] We thank C. Natoli for providing the numerical program, as from C.R.Natoli et al., *Phys. Rev.* **A 22** (1980) 1104.

[23] Z. Kunst, W. J. Stirling, Proc. Large Hadron Collider Workshop, Aachen, 4-9 October 1990.

[24] V.D.Barger and R.J.N.Phillips,*Collider Physics*, Addison- Wesley 1988.

[25] R.Van Royen and V.Weisskopf, *Nuovo Cimento* **50A** (1967) 617.

[26] R.Barbieri, G.Curci, E. d'Emilio and R. Remiddi, *Nuclear Phys.* **B154** (1979) 535.

[27] V.Fadin, V.Khoze and T.Sjostrand, *Zeit Physics* **C48** (1990) 613.

[28] A. Grau and G. Pancheri," *Toponium Production at Hadron Colliders*", The FermiLab Meeting, DPF '92. Batavia, Nov. 10-14 1992. Eds. C.H.Allbright et al.; N.Fabiano, A.Grau and G.Pancheri, " *Toponium Bound States at LHC/SSC*", VIII Corso Invernale di Fisica Adronica, Folgaria 31st January-6 february 1993.

[29] Ll. Ametller, A.Gava, N.Paver and D. Treleani, *Phys. Rev.* **D32** (1985) 1699.

[30] A.W.N.Glover and M.J.J. Van der Bij, *Phys. Lett.* **B206** (1988) 701.

[31] P.Aurenche, A.Douiri, R.Baier, M.Fontannaz and D.Shiff, *Z.Phys.* **C29** (1985) 459.

[32] P.N.Harriman, A.D.Martin, W.G.Sterling and R.G. Roberts, *Phys.Rev.* **D42** (1990) 798.

[33] C. Seez et al., *"Photon Decay Modes of the Intermediate Mass Higgs"*, Proc. Large Hadron Collider Workshop, Aachen, 4-9 October 1990 and private communication.